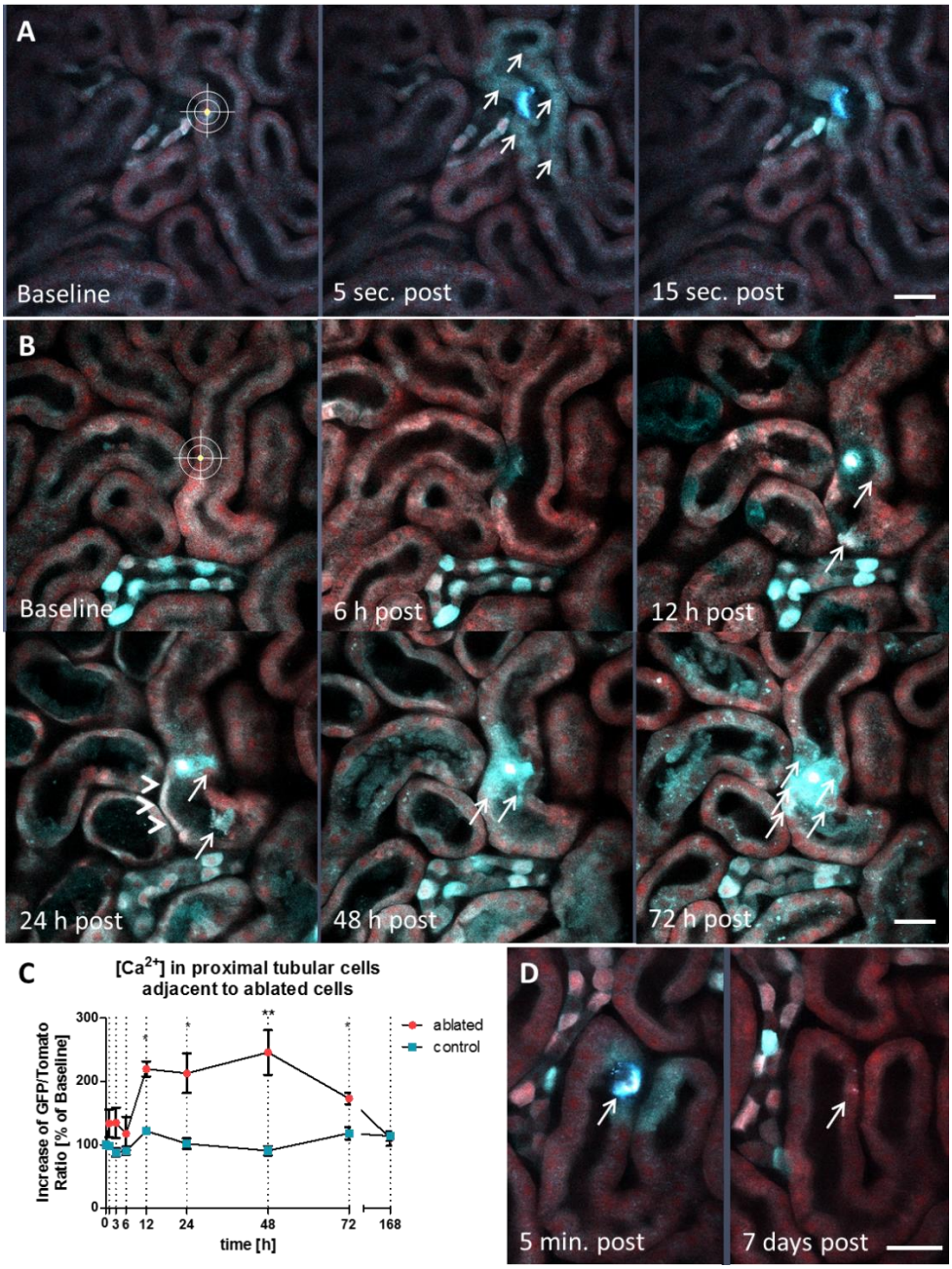

Supplemental figure 1: Proximal tubular intracellular calcium levels are elevated in response to local tubular injury. To investigate proximal tubular [Ca2+] during injury and regeneration, fully induced Pax8-iCre x GCaMP5 mice were used. These mice express the fluorescent calcium indicator protein GCaMP5G (cyan) and tdTomato (red) in all tubular cells. Increases in tubular [Ca2+] lead to a bright GCaMP5G fluorescence (cyan) while tdTomato fluorescence served as fluorescent control. Baseline intravital 2-PM imaging of Pax8-iCre x GCaMP5 kidneys revealed steady [Ca2+] levels in proximal tubules. In contrast, collecting ducts showed single cells with high baseline [Ca2+], which helped to re-identify the same cortical areas over several days in vivo. (A) Laser-induced tubular cell ablation induced a quick and immediate calcium wave over the affected proximal tubular segment (arrows, 5 seconds post injury). 15 seconds post injury, only few cells in the close vicinity showed elevated [Ca2+] levels. Bar=20 µm. (B) In vivo serial 2-PM imaging of the same tubule before and 6, 12, 24, 48 and 72 h after tubular cell ablation. 12 h after laser-induced injury, scattered tubule cells with enhanced [Ca2+] levels were detected within the injured tubule segment (arrows). 24 h post injury, individual cells with increased [Ca2+] levels migrated within the injured tubule segment (arrows) and there was a characteristic flattening of the proximal tubular epithelium in vicinity of the injury site (arrowheads) which was associated with increased [Ca2+] levels. Proximal tubular cell proliferation started 48-72 h after injury (arrows). Bar=20 µm. (C) Proximal tubular [Ca2+] levels of injured and control tubules expressed as changes of GCaMP5G/tdTomato fluorescence ratio of baseline values (n=5 each, * p<.05; ** p<.01 for ablated tubules vs. control tubules). (D) Proximal tubule cells are replaced by cells of tubular origin. 7 days after injury, in vivo lineage tracing using Pax8-iCre x GCaMP5 mice revealed no dilution of tdTomato-positive proximal tubular cells at the injury site (arrows). Bar=20 µm.

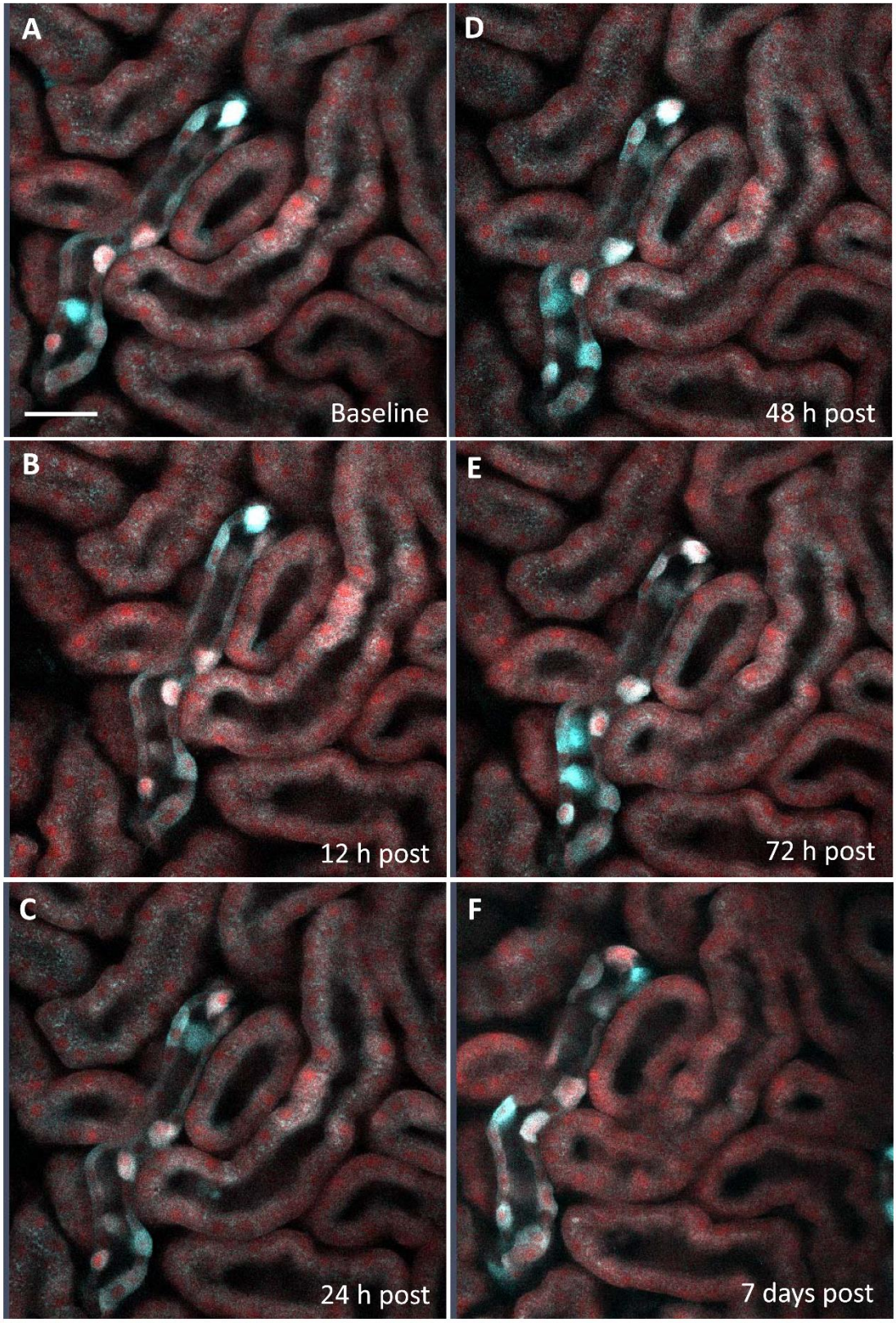

Supplemental figure 2: Proximal tubular intracellular calcium levels are unaltered in control experiments. Serial imaging of fully induced Pax8-iCre x GCaMP5 mice during control conditions. GCaMP5G (cyan) and tdTomato (red) fluorescence remain unchanged after 12 (B), 24 (C), 48 (D), 72 h (E) and 7 days post (F), when compared to baseline conditions (A). Bar=20 µm.

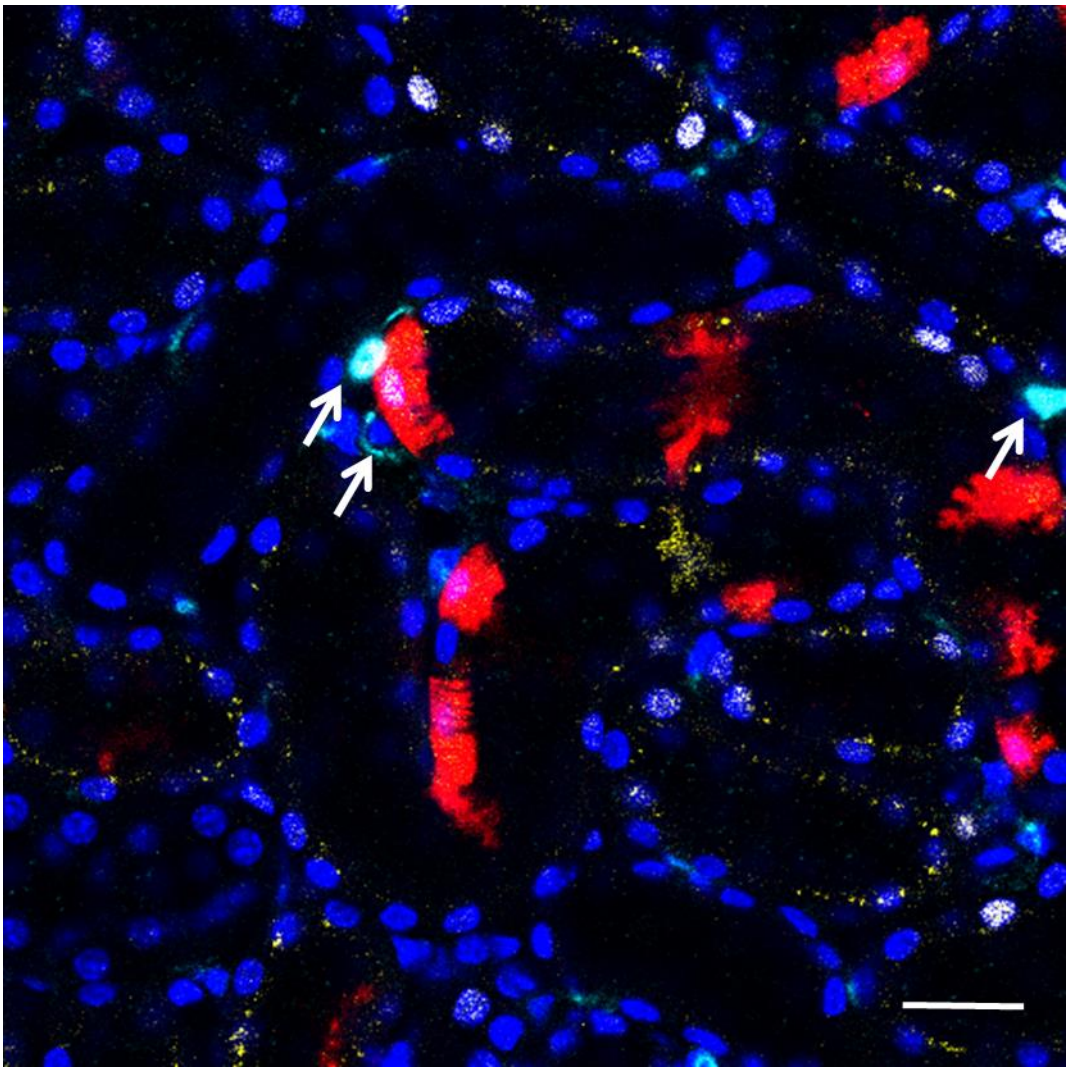

Supplemental figure 3: *Ex vivo* histology of a control Pax8-iCre x Confetti kidney areal. In control experiments, the dedifferentiation marker CD44 (cyan) was only expressed in a few interstitial cells (arrow), but not in the renal epithelium. Bar=20 µm.

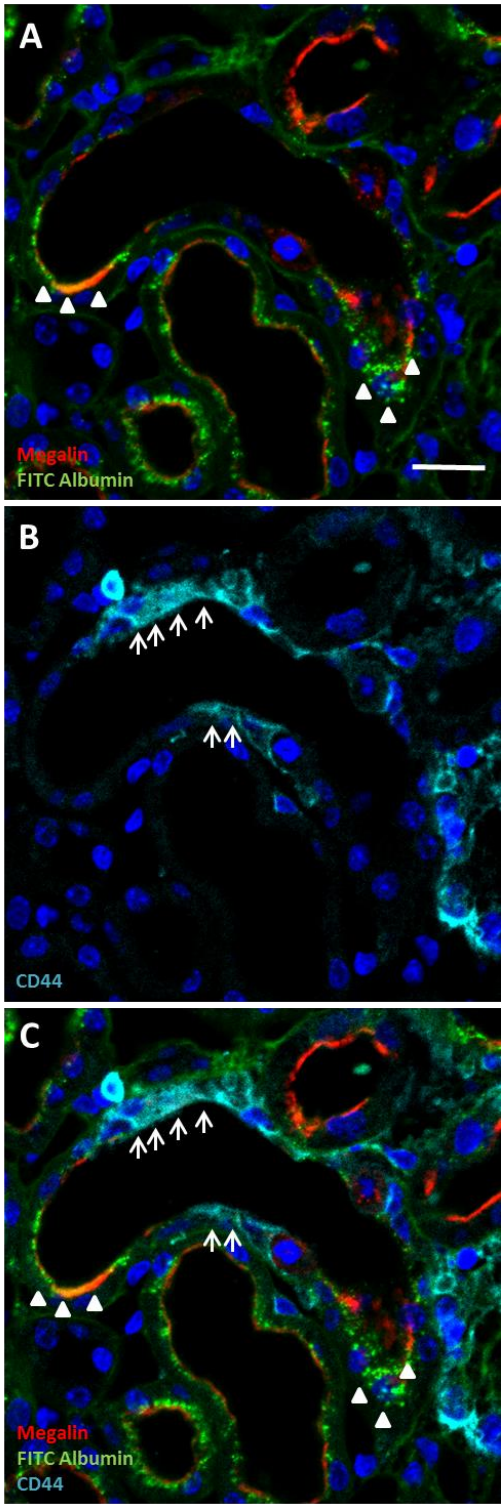

Supplemental figure 4: CD44-positive proximal tubule epithelial cells lack megalin-expression. Analysis of tubular CD44 and megalin expression patterns, 2 days post tubular cell ablation. (A) In vivo injected FITC albumin (green) co-localizes with megalin staining (red, arrowheads). (B) CD44 staining (cyan). (C) CD44 (cyan, arrows) and megalin (red) staining reveal inverse expression pattern Bar=20 µm.

.

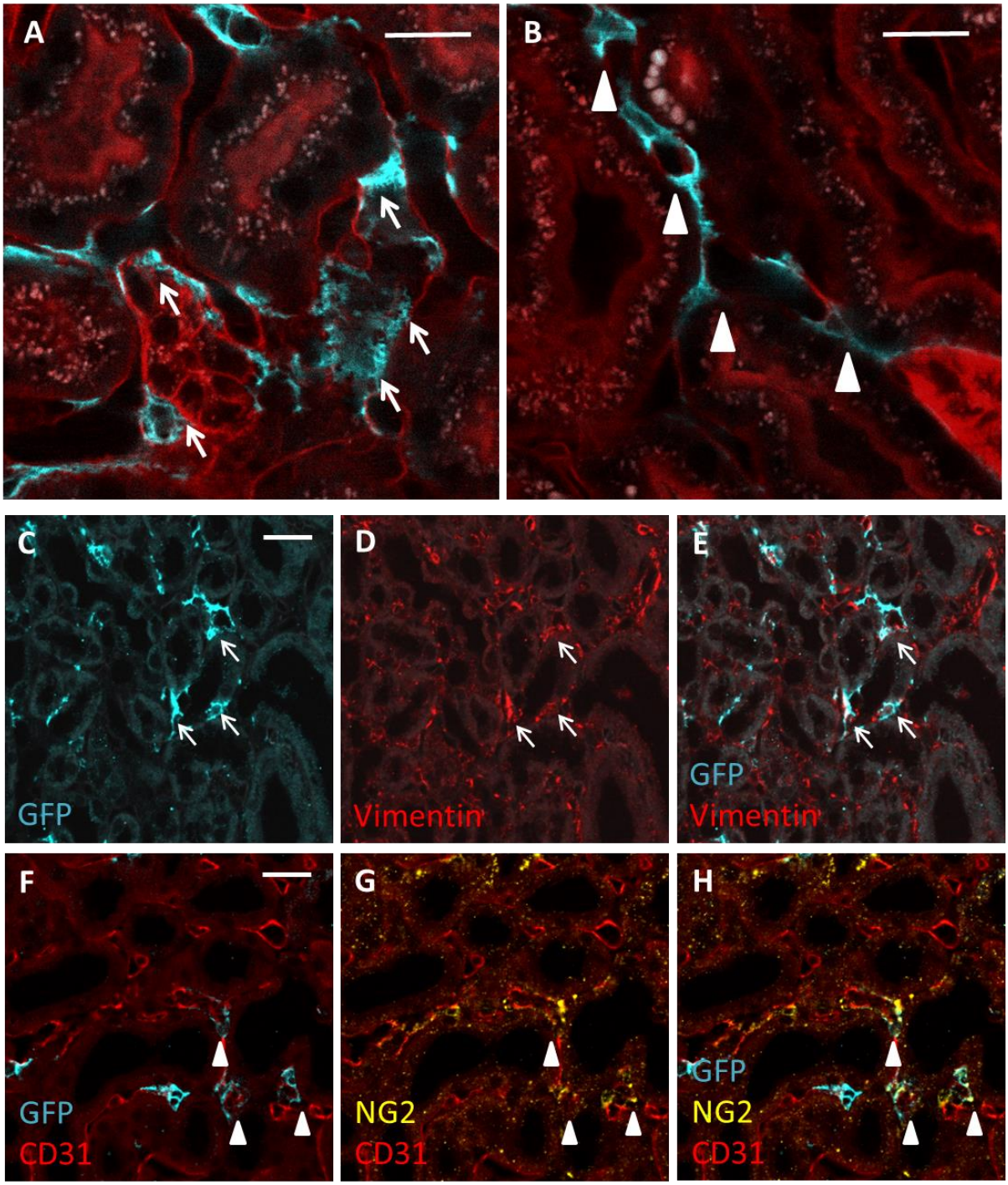

Supplemental figure 5: Characterization of interstitial PDGFRß-positive cells. (A) Using intravital 2-PM imaging of fully induced PDGFRß-iCre x mTmG mice, which express GFP (cyan) in PDGFRß-positive cells and tdTomato in all other cells, we detected two different PDGFRβ-positive cell types. Interstitial fibroblasts were identified by long cell extensions touching the tubular epithelium (A, arrows). In addition, we found PDGFRß-positive pericytes, which were characteristically wrapped around peritubular capillaries (B, arrowheads). bar=20 µm. To further analyze the identity of renal PDGFRß-positive fibroblasts and pericytes, we performed immunostainings of PDGFRß-iCre x mTmG kindey paraffin sections for genetically encoded GFP (cyan), and a co-staining for vimentin as a fibroblast-marker (E, red) and neural/glial antigen 2 (NG2) as a pericyte marker (H, yellow). The peritubular vasculature was identified by CD31 staining (H, red). Bar=20 µm.

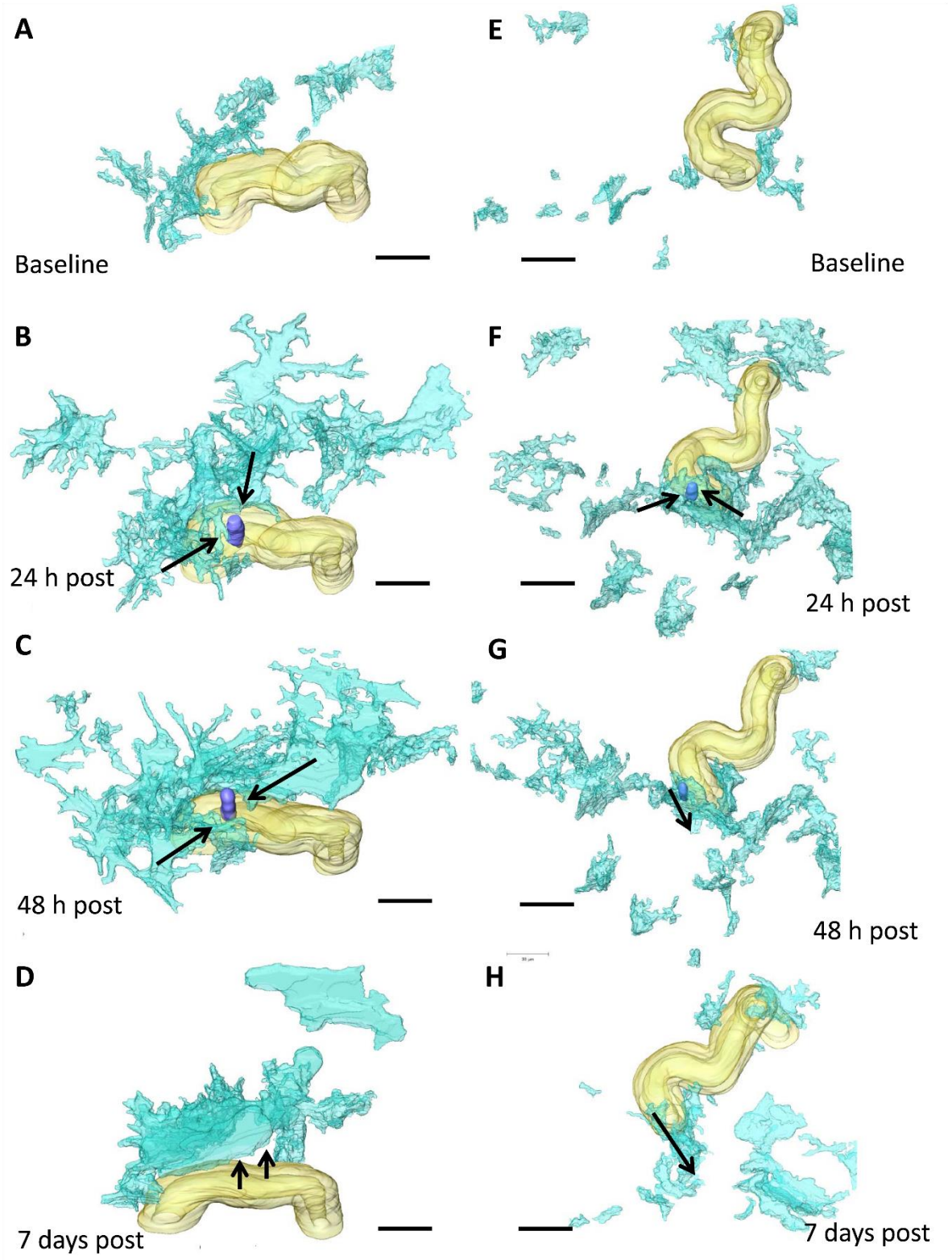

Supplemental figure 6: Interstitial PDGFRß-cells are motile and are recruited to the site of tubular injury. 3-D reconstruction of renal tubules of PDGFRß x mTmG kidneys before (A, E) and 24 (B, F), 48 h (C, G) and 7 days (D, H) after laser-induced tubular cell ablation. Interstitial PDGFRβ-cells (cyan) were quickly recruited (arrows) towards the site of injury (purple) and wrapped around the affected tubular epithelium within 24-48 h. 7 days post, they redistribute into the renal interstitium.

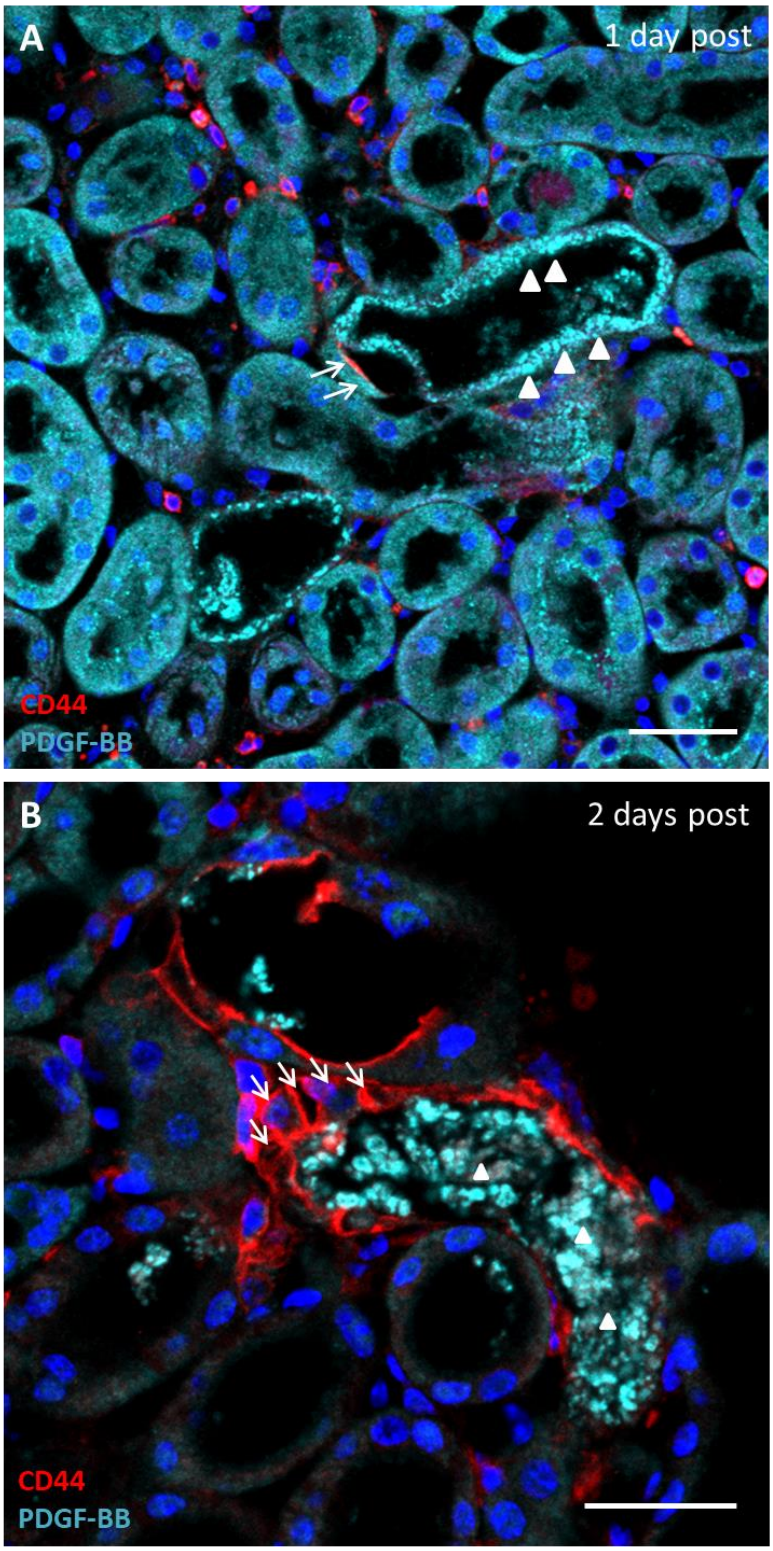

Supplemental figure 7: Tubular cells express higher PDGF-BB level 1 day after tubular cell ablation. (A) PDGF-BB-staining (cyan) 1 day after tubular cell ablation reveals higher expression levels at injured tubule segment (arrowheads). when compared to uninjured tubules. Note that early epithelial CD44-expression (red) is associated with the shedding of apical tubular cell material into the tubular lumen. This is consistent with the loss of the apical tubular brushborder during tubule cell dedifferentiation. (B) 2 days post tubular cell ablation, dedifferentiation of the injured tubule is indicated by strong epithelial CD44-expression (red, arrows). Furthermore, the apical broshborder had been shedded into the tubular lumen and the dedifferentiated tubule lost its PDGF-BB content. Note the lack of cyan PDGF-BB-staining in the epithelium and the accumulation of PDGF-BB-positive tubular material in the tubule lumen (arrowheads), indicating the shedding of Bar=20 µm for each panel.

Supplemental movie 1: Z-stack through the renal cortex of an induced PDGFRß x mTmG mouse. Note the spine-like character of GFP-positive PDGFRß-cells (green) connecting individual cells and the tubular epithelium.

Supplemental methods

Animals. Both male and female mice at the age of 6-12 weeks were randomly included into the experiments. To study the dynamics of proximal tubular cell regeneration and dynamics, Pax8-iCre x Confetti and Pax8-iCre x GCaMP5 mice were generated by crossing mice expressing the inducible Cre recombinase under the control of the Pax8 promotor (B6.Cg-Tg(Pax8-rtTA2S*M2)1Koes/J) (Traykova-Brauch, Schonig et al. 2008) with either R26RConfetti (Gt(ROSA)26Sortm1(CAG-Brainbow2.1)Cle/J) (Snippert, van der Flier et al. 2010) or PC-G5-tdT (B6;129S6-Polr2atm1(CAG-GCaMP5g,-tdTomato)Tvrd/J) (Gee, Smith et al. 2014) mice respectively. After induction of the Cre-recombinase with doxycycline, Pax8-iCre x Confetti mice express either CFP, GFP, YFP or RFP in tubular cells and allow cell fate tracing. Doxycycline-induced Pax8-iCre x GCaMP5 mice co-express the fluorescent calcium indicator protein variant GCaMP5G and tdTomato red fluorescent protein in tubular cells. To study interstitial fibroblasts in the context of kidney regeneration, PDGFRß-iCre x mTmG and PDGFRß-iCre x GCaMP5, were generated by crossing PDGFRß-iCre mice (B6.Cg-Tg(Pdgfrb-cre/ERT2)6096Rha/J) (Foo, Turner et al. 2006) with either Rosa mTmG (Gt(ROSA)26Sortm4(ACTB-tdTomato,-EGFP)Luo/J) (Muzumdar, Tasic et al. 2007) or the above mentioned PC-G5-tdT mice, respectively. After tamoxifen-induced Cre recombinase-expression under the control of the PDGFRß promotor, PDGFRß-positive cells expressed either GFP (PDGFRß-iCre x mTmG mice) or GCaMP5G and tdTomato (PDGFRß-iCre x GCaMP5 mice). To detect renal proliferative cells in vivo, we used CyclinB1-GFP reporter mice (Tg(Pgk1-Ccnb1/EGFP)1Aklo/J). All animals were purchased from Jackson Laboratory (Bar Harbor, ME) and genotyping was conducted according to the guidelines provided by Jackson Laboratory. Genotyping of PDGFRß-iCre was done using primers for general Cre detection (Cre sense 5'-cag aac ctg aag atg ttc-3' Cre antisense 5'-caa gat tac gta tat cc-3').

Cre recombinase-induction by doxycycline or tamoxifen. To fully induce Cre recombinase under the control of the Pax8 promotor, Pax8-iCre x GCaMP5 mice received doxycycline (Panreac Applichen) in the drinking water for one week (2 g doxycycline/L, 5% saccharose). Before performing the experiments, a 2-week wash-out period was granted to ensure doxycycline was fully removed from the organism of the mice. For partial induction of Pax8-iCre recombinase, Pax8-iCre x Confetti mice were given a single oral doxycycline administration (0.6 mg/kg BW) by gavage followed by a 2-week wash-out period. This induced a scattered expression of either CFP, GFP, YFP or RFP in only few tubular cells to allow single cell fate tracing.

To achieve full induction in PDGFRß-iCre reporter models (PDGFRß-iCre x mTmG/GCaMP5 mice), tamoxifen (Cayman Chemical Company) was orally given on three days, followed by a one day recovery period after each administration (0.2 mg/kg BW per gavage, each). Subsequently a two week wash-out period was granted to clear tamoxifen from the organism.

Serial intravital multiphoton imaging using the abdominal imaging window technique. To investigate structural and functional changes of the renal cortex of living mice over time, we performed serial multiphoton imaging using the abdominal imaging window (AIW) technique (Ritsma, Steller et al. 2013). To facilitate consecutive imaging of the same cortical kidney regions over days a polyethylene glycol-coated, cover-slipped titanium ring was implanted into the abdominal wall as described before (Ritsma, Steller et al. 2013). Briefly, mice received buprenorphine [0.1 mg/kg BW, s.c.] prior to surgery on an operating table with a servo-controlled heating plate under isoflurane-mediated anesthesia [1.5 vol. %]. Under sterile conditions, a 1 cm long dorsoventral incision is placed above the left kidney which is then surrounded by a purse-string suture attaching the skin to the muscle layer of the abdominal wall. The kidney is then glued to the glass front of a sterile, cover-slipped titanium ring (12 mm

diameter), which is inserted into the abdominal wall and fixed by closure of the purse-string suture. After recovery from the surgery, the AIW serves as a temporary window into the living kidney of the mouse and allows the investigation of structural and functional changes during renal injury and regeneration.

Intravital multiphoton imaging of the kidney was performed as described before (Schiessl, Bardehle et al. 2013, Schiessl and Castrop 2013, Schiessl, Kattler et al. 2015, Schiessl, Hammer et al. 2016). The mice were anaesthetized with 1.5 vol. % isoflurane and placed on an inverted Zeiss LSM 710 NLO confocal fluorescence microscope (Carl Zeiss), which was equipped with a servo-controlled warming plate to maintain the body temperature of the mice at 37°C. Visualization of the kidney was provided through the implanted AIW using a 40 x long distance (LD) C Apochromat 40/1.1 water objective. Excitation of Pax8-iCre x GCaMP5 and PDGFRß-iCre x GCaMP5/mTmG kidneys was achieved using a Chameleon Ultra-II multiphoton laser (Coherent) at 860 nm. Fluorescent emission was collected using Zeiss BIG non-descanned detectors equipped with a longpass XR 560 filter, separating light for the detection with filterset 1 (GFP, GCaMP5G, FITC): 525/50 ET bandpass filter and filterset 2 (tdTomato): 630/75 ET bandpass filter. Excitation of Pax8-iCre x Confetti mice was achieved by consecutive scanning using 800 nm (CFP excitation), 940 nm (GFP and YFP excitation) and 1040 nm (RFP excitation) (Hackl, Burford et al. 2013). Fluorescent emission was detected using non-descanned detectors equipped with a longpass 490 and shortpass 485 IR+ filter for CFP, a longpass 514 filter combined with a 504/12 bandpass filter for GFP and using a non-descanned Zeiss BIG detector equipped with a longpass XR 560 filter followed by a 535/30 ET bandpass filter for YFP- and a 630/75 RT bandpass filter for RFP-detection respectively.

Mice were either subject to short-term serial imaging: 0 h, 1 h, 3 h, 6 h, 12 h, 24 h post tubular cell ablation or long-term serial imaging: 0 h, 24 h, 48 h, 72 h, 164 h post tubular cell ablation. Individual imaging sessions did not exceed 30 minutes at a time and were followed

by a 30 minutes observation and recovery period, in which the mice were kept in a separate cage on a heating pad.

Laser-induced tubular cell ablation. To mimic the loss of single tubular cells in the healthy kidney, we ablated single proximal tubule cells by high laser exposure. Proximal tubules were identified by characteristic autofluorescence, which also allowed to distinguish between S1 and S2 segments as described before (Hato, Winfree et al. 2017). This study mainly focused on the regenerative capacity of proximal tubule S1 segments. S1 segment identity was further confirmed by in vivo injected FITC albumin injection. After baseline recordings of the area of interest, this was achieved by targeting a single cell with maximum zoom and 30 % laser excitation (860 nm) for two seconds. The injured kidney cortex area was then subject to serial imaging as described above to investigate epithelial and interstitial regenerative actions.

Determination of cell migration and proliferation. To determine structural changes of tubular and interstitial cells in response to tubular cell ablation, the same cortical regions in the kidney were subject to optical sectioning (z-stacks) with a total z-depth of 25 µm in 1 µm steps. Structural changes over time, such as tubular or PDGFRß-cell migration were then detected in a side-by-side fashion in addition to 3-D reconstruction of the z-stacks using Amira 5.3 (Visage Imaging). Quantification of cell migration was conducted in a simplified manner, including only migration in the x/y plane, using the ZEN2010 software.

To detect tubular cell proliferation in Pax8-iCre x Confetti mice, we co-injected Hoechst 33324 [25 µl of a 10 mg/ml solution, Thermo Fischer] to label cell nuclei. Z-stacks of baseline conditions and 7 days after tubular cell ablation were then subject to 3-D reconstruction using Amira 5.3 and proliferation was expressed as the increase of Hoechst-labeled nuclei associated with monochromatic areas in the injured epithelium. In addition, we used CyclinB1-GFP reporter mice, which express GFP in replicating cells during S, G2 and M stages of the cell cycle.

Intracellular calcium measurement. Changes of intracellular changes of calcium in tubular and interstitial cells were detected using either Pax8-iCre x GCaMP5 or PDGFRß-iCre x GCaMP5 mice respectively, which co-express the fluorescent calcium indicator GCaMP5G in addition to tdTomato. Changes of intracellular calcium values were expressed in a ratiometric fashion by normalizing the acquired fluorescence intensity values for GCaMP5G (subject to fluctuation determined by intracellular calcium levels) over the values measured for tdTomato (fluorescence intensity independent of calcium) at a given time. In detail, GCaMP5G/tdTomato imaging of the same cortical areas in the kidney were conducted as a time lapse of 5 images for each experimental timepoint. The fluorescent intensity of GCaMP5G and tdTomato (determined from five images per timepoint) was averaged from 5 images by placing regions of interest in tubular/PDGFRß-positive cells and then used for ratiometric calculation. Changes of GCaMP5G/tdTomato fluorescent intensity ratio were determined from paired observations and expressed in % of the baseline values.

Determination of proximal tubular function. To assess proximal tubular function during tubular injury and regeneration, we injected FITC-conjugated albumin to investigate proximal tubular albumin-endocytosis of the injured epithelium in vivo. FITC-conjugated albumin (40 µl of a 40 mg/ml solution, Sigma) was administered by tail vein injection prior to intravital imaging of the kidney for each investigated timepoint. FITC albumin-fluorescence intensity was then measured on the apical side of the affected tubular epithelium before and 24, 48, 72 and 164 h after laser-induced cell ablation. The same protocol was followed for unaffected control proximal tubules in remote distance to the injury side for each time point. Proximal tubular albumin-endocytosis before and after tubular injury was then expressed in percent of control tubular FITC albumin-fluorescence.

Immunohistochemistry and ex vivo histology. Animals were perfused with 3% paraformaldehyde solution in phosphate buffered saline (pH 7.2) at a constant perfusion

pressure of 130 mm Hg. Subsequently, the fixed kidneys were processed for paraffin sections by incubation in ascending alcohol solutions (70, 80, 90, and 100% methanol), followed by 100% isopropanol for 2x30 minutes each. The tissue was then incubated in 50% isopropanol in paraffin at 70°C before embedding in paraffin. Areas from the middle of the kidney were sliced (5 µm) and blocked with 10% horse serum (HS)/1% bovine serum albumin (BSA)/PBS for 20 minutes at room temperature. Sections were then incubated with the first antibody overnight (4°C). Following three washing steps (PBS), the secondary antibodies (diluted 1:400 in 1% BSA) were applied for 90 minutes at room temperature and the sections were then mounted with Dako Mounting Medium (Agilent), before imaging on the Zeiss LSM 710 confocal microscope. The following primary antibodies were used: rat anti-CD44 IgG (1:100, BD Pharmingen), guinea pig anti-megalin IgG (1:100, kindly provided by Franziska Theilig, Ph.D.), goat anti-Vimentin IgG (1:100, Santa Cruz Biotechnology), mouse anti-alpha SMA IgG (1:600, Abcam), rabbit anti- PDGF-BB IgG (1:400, Abcam), rabbit anti-PDGFRß IgG (1:200, Abcam), chicken anti-GFP IgY (1:600, Abcam), goat anti- albumin (1:400, Abcam).

As secondary antibodies for immunostainings, either Cy5-conjugated donkey anti-rabbit IgG (Jackson ImmunoResearch), Cy5-conjugated donkey anti-rat IgG (Jackson ImmunoResearch), Cy5-conjugated donkey anti-mouse IgG (Jackson ImmunoResearch), Cy5-conjugated donkey anti-goat IgG (Jackson ImmunoResearch), TRITC-conjugated donkey anti-goat IgG (Jackson ImmunoResearch), TRITC-conjugated donkey anti-chicken IgG (Jackson ImmunoResearch), Cy3-conjugated donkey anti-guinea pig IgG (Jackson ImmunoResearch), Cy2-conjugated donkey anti-rat IgG (Jackson ImmunoResearch), Cy2-conjugated donkey anti-mouse IgG (Jackson ImmunoResearch), Cy2-conjugated donkey anti-goat IgG (Jackson ImmunoResearch), or Cy2-conjugated donkey anti-guinea pig IgG (Sigma-Aldrich) were used.

To analyze if laser-induced tubular cell ablation induced dedifferentiation of resident tubular epithelial cells we stained for the dedifferentiation marker CD44. To investigate the

same cortical kidney regions, which had been subject to serial imaging in vivo, we established *ex vivo* histology. Subsequently to in vivo serial imaging, PDGFRß-iCre x mTmG or Pax8-iCre x Confetti mice were fixed with 3% paraformaldehyde either at day 1, 2 or 7 after laser-induced cell ablation. Next, the cortical renal area which was attached to the abdominal imaging window, was separated as a 1-2 mm thick tissue section. The recovered tissue was washed twice in PBS for 15 minutes, followed by blocking in 1% BSA and 10 % HS for 1 h. Primary antibody (rat anti CD44, BD Pharmingen, 1:100 in 1% BSA 10% HS) was then incubated over night at 4 °C. Subsequently to washing with 1% BSA the secondary antibody (Cy5-conjugated donkey anti-rat, Jackson ImmunoResearch, 1:400 in 1%BSA) was incubated for 4 h. After washing with PBS the tissue section was then embedded in PBS between two coverslips separated by a 1-2 mm thick spacer (SunJim Lab). The embedded and stained tissue section was then investigated using confocal microscopy (Zeiss LSM 710). Endogenous fluorescence of genetically expressed fluorescent proteins was not affected by the staining protocol. This enabled the identification of the same cortical areas that were subject to serial imaging in vivo.

CLARITY. To further investigate interstitial PDGFRß-cell morphology in the kidney cortex, we performed CLARITY of fully induced PDGFRß-iCre x mTmG mice as described before (Tomer, Ye et al. 2014). Briefly, the mice were perfused with hydrogel monomer solution (1% acrylamide, 0.025% bisacrylamide, 4% PFA/PBS with 0.25% VA-044 initiator, Wako). Organs were removed and placed in the hydrogel monomer solution for 2 days. Polymerization was achieved at 37°C for 4 h after removing oxygen from the solution using nitrogen. The tissue was then subject to passive clarity by incubation in 4% SDS, 200 mM boric acid for three weeks at 37°C.

Trapidil-treatment. To investigate the role of PDGF-BB and PDGFRß-signalling in PDGFRß-cell activation and recruitment, we inhibited PDGFRß in vivo using the competitive inhibitor trapidil (Sigma). Trapidil was dissolved in sterile saline at 10 mg/ml and was

administered i.p. to PDGFRß-iCre x mTmG and PDGFRß-iCre x GCaMP5 mice [60 mg/kg, 3 times/day].

Statistical analysis. Data were analyzed by ANOVA with Bonferroni post hoc test using Graph Pad Prism 5 (GraphPad Software, La Jolla, CA). All data are given as means ± SEM. $P<.05$ was considered significant.

Study approval. Animal care and experiments were approved by the local government, Regierung der Oberpfalz, and carried out in accordance with National Institutes of Health principles as outlined in the Guide for the Care and Use of Laboratory Animals.

References of suppl. information:

Foo, S. S., C. J. Turner, S. Adams, A. Compagni, D. Aubyn, N. Kogata, P. Lindblom, M. Shani, D. Zicha and R. H. Adams (2006). "Ephrin-B2 controls cell motility and adhesion during blood-vessel-wall assembly." Cell **124**(1): 161-173.

Gee, J. M., N. A. Smith, F. R. Fernandez, M. N. Economo, D. Brunert, M. Rothermel, S. C. Morris, A. Talbot, S. Palumbos, J. M. Ichida, J. D. Shepherd, P. J. West, M. Wachowiak, M. R. Capecchi, K. S. Wilcox, J. A. White and P. Tvrdik (2014). "Imaging activity in neurons and glia with a Polr2a-based and cre-dependent GCaMP5G-IRES-tdTomato reporter mouse." Neuron **83**(5): 1058-1072.

Hackl, M. J., J. L. Burford, K. Villanueva, L. Lam, K. Susztak, B. Schermer, T. Benzing and J. Peti-Peterdi (2013). "Tracking the fate of glomerular epithelial cells in vivo using serial multiphoton imaging in new mouse models with fluorescent lineage tags." Nat Med **19**(12): 1661-1666.

Hato, T., S. Winfree and P. C. Dagher (2017). "Intravital imaging of the kidney." Methods **128**: 33-39.

Muzumdar, M. D., B. Tasic, K. Miyamichi, L. Li and L. Luo (2007). "A global double-fluorescent Cre reporter mouse." Genesis **45**(9): 593-605.

Ritsma, L., E. J. Steller, S. I. Ellenbroek, O. Kranenburg, I. H. Borel Rinkes and J. van Rheenen (2013). "Surgical implantation of an abdominal imaging window for intravital microscopy." Nat Protoc **8**(3): 583-594.

Schiessl, I. M., S. Bardehle and H. Castrop (2013). "Superficial nephrons in BALB/c and C57BL/6 mice facilitate in vivo multiphoton microscopy of the kidney." PLoS One **8**(1): e52499.

Schiessl, I. M. and H. Castrop (2013). "Angiotensin II AT2 receptor activation attenuates AT1 receptor-induced increases in the glomerular filtration of albumin: a multiphoton microscopy study." Am J Physiol Renal Physiol **305**(8): F1189-1200.

Schiessl, I. M., A. Hammer, V. Kattler, B. Gess, F. Theilig, R. Witzgall and H. Castrop (2016). "Intravital Imaging Reveals Angiotensin II-Induced Transcytosis of Albumin by Podocytes." J Am Soc Nephrol **27**(3): 731-744.

Schiessl, I. M., V. Kattler and H. Castrop (2015). "In vivo visualization of the antialbuminuric effects of the angiotensin-converting enzyme inhibitor enalapril." J Pharmacol Exp Ther **353**(2): 299-306.

Snippert, H. J., L. G. van der Flier, T. Sato, J. H. van Es, M. van den Born, C. Kroon-Veenboer, N. Barker, A. M. Klein, J. van Rheenen, B. D. Simons and H. Clevers (2010). "Intestinal crypt

homeostasis results from neutral competition between symmetrically dividing Lgr5 stem cells." Cell **143**(1): 134-144.

Tomer, R., L. Ye, B. Hsueh and K. Deisseroth (2014). "Advanced CLARITY for rapid and high-resolution imaging of intact tissues." Nat Protoc **9**(7): 1682-1697.

Traykova-Brauch, M., K. Schonig, O. Greiner, T. Miloud, A. Jauch, M. Bode, D. W. Felsher, A. B. Glick, D. J. Kwiatkowski, H. Bujard, J. Horst, M. von Knebel Doeberitz, F. K. Niggli, W. Kriz, H. J. Grone and R. Koesters (2008). "An efficient and versatile system for acute and chronic modulation of renal tubular function in transgenic mice." Nat Med **14**(9): 979-984.